MOLECULAR PHYSICS, 1999, VOL. 96, NO. 3, 371–379

Quantum monodromy in the spectrum of H_2O and other systems: new insight into the level structure of quasi-linear molecules

M. S. CHILD[1], T. WESTON[1] and J. TENNYSON[2],
[1]Physical and Theoretical Chemistry Laboratory, South Parks Road, Oxford OX1 3QZ, UK
[2]Department of Physics and Astronomy, University College London, Gower Street, London WC1E 6BT, UK

(*Received 1 April 1998; revised version accepted 16 June 1998*)

The concept of quantum monodromy is introduced to give insight into the energy levels of systems with cylindrically symmetrical potential energy barriers. The κ structure of bending progressions of bent molecules and the pendular states of dipolar molecules in strong electric fields are taken as molecular examples. Results are given for a two-dimensional champagne bottle model, for six computed bending progressions for water taken from the compilation of Partridge and Schwenke and for the quantal spherical pendulum. Sharp changes in the energy level patterns around the barrier energy are related to changes in the forms of the relevant classical trajectories. Analytical insight into the mathematical origin of the monodromy are also given.

1. Introduction

The concept of monodromy (meaning 'once round') is well established in the mathematical literature [1, 2]. One type of physical application occurs in any time periodic system, where for example the stabilities of fixed points in the period map (or Floquet map) are characterized by the eigenvalues of the monodromy matrix [3]. Another type of application comes from the classical mechanical literature [4], where it is used to demonstrate a gross topological obstruction to the global construction of angle–action variables. Translated into quantum mechanical language, this implies the absence of any smoothly valid set of quantum numbers for the entire spectrum. The quantum monodromy of the present paper is employed in the latter sense. Specifically it is shown, by semiclassical arguments, to be a generic property of any system with a cylindrically symmetrical potential barrier. A graphical illustration of the lack of connectivity is shown in figure 1 below. Molecular illustrations are given for the bending–rotating states of H_2O and for the pendular states of dipolar molecules in strong electric fields [5].

It has of course been known since the early papers of Dixon [6] and Johns [7] on the spectroscopy of quasi-linear molecules that the states below the barrier to linearity are conveniently labelled by bent molecule quantum numbers $|v_2, \kappa\rangle$ and those above by linear molecule ones, say $|n_2, \ell\rangle$†; but it is less often noted that the algebraic relations $\ell = \kappa$ and $n_2 = 2v_2 + |\ell|$ between the two sets imply that both designations are equally valid for any particular energy state. The monodromy provides an elegant test for the smoothness of either of these individual labelling schemes (and of any other scheme) by tracing out a circle in energy and angular momentum space around a 'critical point' at the barrier energy with $\kappa = \ell = 0$. At the same time it brings out a sudden change in the energy dependence on either $|v_2, \kappa\rangle$ or $|n_2, \ell\rangle$ when crossing the barrier to linearity, which is reflected for example in the abrupt halving of the apparent bending vibrational frequency in the photoelectron spectrum of H_2S [8].

The existence of such abrupt changes is not of course new. In particular Dixon [6] drew attention to the presence of a sharp dip in the local vibrational level spacing at $\kappa = 0$ at the barrier to linearity, which is smoothed away as κ increases. The resulting local convergence of the low κ levels certainly implies a reorganization of the energy level pattern around the barrier maximum, but

† n_2 in this notation corresponds to v_2^{linear} of Johns [7]. There is also a spectroscopic convention to use k for the signed value of κ, but in the absence of similar conventions for ℓ and later m (for the pendular states) it is less confusing in the present context to treat κ, ℓ and m as signed quantities.

the precise consequences for the energy variation at fixed v_2 or n_2 have not previously been discussed. Nor has the generality of the phenomenon been determined by reference to the equally abrupt changes in the nature of the classical trajectories.

Previous work on the vibrational–rotational structures of Renner–Teller systems may also be mentioned. For example Jungen and Merer [9] show that the computational equivalence of the κ and ℓ bases is broken by the presence of Renner–Teller coupling. The influence of this coupling on the rate of switch-over from bent to linear patterns has also been discussed [10, 11], with particular reference to the spectrum of H_2S^+ [12]. The present paper deals however only with motions on a single potential energy surface. Its novel conceptual aspects relate (a) to the absence of connectivity in either the $|v_2, \kappa\rangle$ or $|n_2, \ell\rangle$ labelling schemes and (b) to the semiclassical origin of abrupt changes in the energy level patterns around the barrier maximum.

The monodromy is introduced in section 2 by reference to a two-dimensional champagne bottle model that was presented in mathematical detail elsewhere [13]. The main purpose of the paper is however to demonstrate that it also persists in the fully coupled vibrational spectrum of H_2O even when the stretching modes are also excited. Results are presented for several calculated bending progressions up to total energies of $28\,000\,cm^{-1}$ on the accurate potential energy surface of Partridge and Schwenke [14]. The monodromy is clearly apparent for (v_1, v_2, v_3) bending progressions with $v_1 + v_3 \leq 2$ although there are some assignment ambiguities at high v_2, particularly for $(v_1, v_3) = (2, 0)$ and $(1,1)$. The generality of the effect is further demonstrated by giving results for the spherical pendular states of a dipolar molecule in a strong electric field. The relevant angular momentum is then the projection m in the field direction while a quantum number v_θ, which counts the nodes in the θ direction, plays the role of v_2. The convenient labelling schemes are $|n, m\rangle$, with $n = 2v_\theta + |m|$, for the low-lying near harmonic states and $|j, m\rangle$ with $j = v_\theta + |m|$, for the high-lying near free rotor states. Each shows the same qualitative monodromic pattern as the previous bending–rotating states.

Section 3 summarizes the main conclusions of an earlier semiclassical analysis of the champagne bottle model [13] and indicates their extensions to the spherical pendulum. The conclusions are summarized and discussed in section 4. Finally interested readers are referred to the appendix on analytical aspects of the monodromy.

2. Quantum monodromy

The origin of the term monodromy is illustrated in figure 1 which shows the central part of a lattice of quantum eigenvalues for the scaled champagne bottle

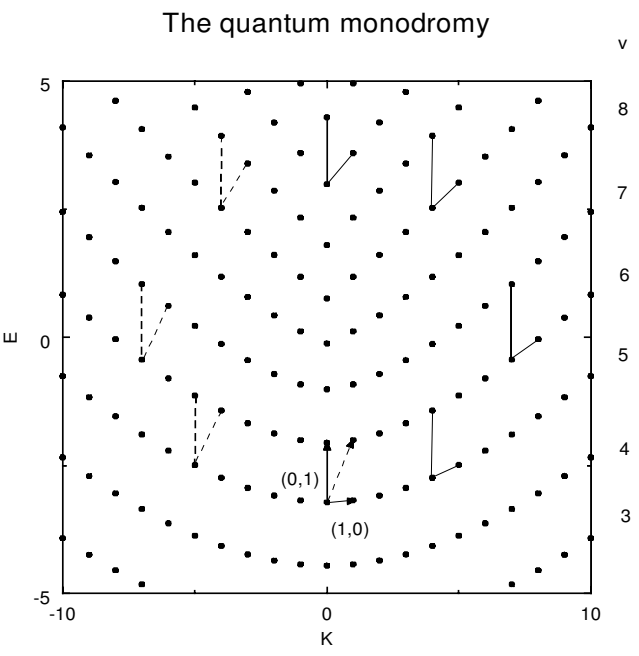

Figure 1. The central part of the computed quantal spectrum for the scaled champagne-bottle model with $\beta = 0.006\,25$. The scaling relations are given after equation (A 2).

Hamiltonian described in the appendix. Each point is labelled by the conserved angular momentum κ and a vibrational quantum number v which increases from zero up each vertical (constant κ) ladder. The monodromy is associated with the non-connectivity of this labelling scheme, due to the presence of a so-called critical point with zero-angular angular momentum at the top of the potential maximum ($E = 0$ in this model). Consider for example the arrowed unit cell with axes $(\Delta\kappa, \Delta v) = (1,0)$ and $(0,1)$ in the lower part of the figure, and follow the smooth evolution of this cell on an anticlockwise circuit around the critical point. The vector $(0,1)$ returns to itself but $(1,0)$ returns to $(1,1)$—both being related to their initial forms by

$$\begin{pmatrix} \Delta\kappa' \\ \Delta v' \end{pmatrix} = \begin{pmatrix} 1 & 0 \\ 1 & 1 \end{pmatrix} \begin{pmatrix} \Delta\kappa \\ \Delta v \end{pmatrix}. \qquad (1)$$

Equation (1) or its inverse for clockwise transport may be verified to apply to the circuit of any vector around the critical point. The conclusion is that (v,κ) may provide local labels for individual quantum states but that the resulting scheme is not smoothly connected over the whole lattice.

Further insight is obtained by noting that points in the upper part of figure 1 are roughly interleaved in successive vertical columns, which means that the energy differences corresponding to $\Delta v = \pm 1$ are roughly half those corresponding to $\Delta\kappa = \pm 1$. In

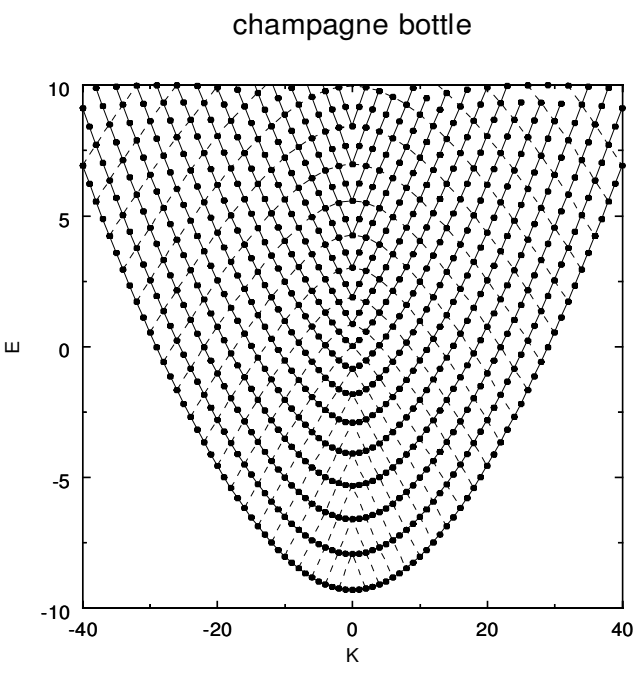

Figure 2. The computed quantal spectrum for the scaled champagne-bottle model with $\beta = 0.00625$. Points indicate the computed eigenvalues. Solid and dashed lines join those with common values of the bent molecule quantum number v and the linear molecule number $n = v + |K|$ respectively. Note the abrupt transition from smooth to kinked variations in both sets of curves around the critical point at $K = 0$, $E = 0$.

other words there is an approximate 2:1 resonance which may be characterized by the quantum number $n = 2v + |K|$, which is of course the linear molecule quantum number of Johns [7]. It is also normal to replace K by ℓ in the labelling of linear states. Figure 2 demonstrates some interesting symmetries between these two $|v, K\rangle$ and $|n, \ell\rangle$ (with $\ell = K$) labelling schemes, by use of continuous and dashed curves to join points with common v and common n values respectively. The smooth roughly quadratic energy variation with K at fixed v in the lower part of the figure goes over to a succession of sharp kinks around $K = 0$ for energies above the critical point. Conversely the dashed curves are roughly quadratic in ℓ or K for $E > 0$ but become kinked for $E < 0$. These features are related in section 3 to the forms of the positive and negative energy trajectories, by use of the Bohr quantization rule.

Similar features are shown in figure 3 for the energies of the $K_a = J$ levels of a variety of computed bending progressions of water. These energy levels were taken from Partridge and Schwenke [14] who computed them on a very accurate spectroscopically determined potential energy surface and also gave a very large number of computer generated assignments. K_a is not of course a rigorous quantum number for H_2O (nor indeed is v_2 except as a counting number) but close symmetric top like degeneracies are expected for high J and K_a. Moreover even the 1_{10} to 1_{11} rotational energy splittings in the known bands are too small to be resolved on the scale of figure 3. The plotted points were therefore taken as Partridge and Schwenke's [14] J_{J0} energy levels for the relevant bending progression.

The lines drawn in figure 3 link the solid points with common v_2 (solid lines) and n_2 (dashed lines) as for figure 2. In some cases it was necessary to reassign the counting number v_2 and these points have a superimposed cross (+). The open points at relatively high levels of vibrational excitation, which are not joined by lines, fall outside the (v_2, K_a) pattern and are usually supernumerary to it. We believe that these levels only appear here due to problems with the automatic assignment procedure employed by Partridge and Schwenke [14]; in many cases they are alternatives to those given by the solid circles. These problems with automatic assignment have been previously discussed [15,16]. It should also be noted that possible high energy anomalies for the $(2, v_2, 0)$ and $(1, v_2, 1)$ progressions have been omitted by truncating the diagrams.

Nevertheless, the qualitative similarity between figure 2 and the various panels of figure 3 is remarkable. The simple quartic minus quadratic champagne bottle model is of course inadequate to account even for a bending cut through the full potential energy surface, but the qualitative features of the diagram depend solely on the existence of a cylindrically symmetric potential maximum at the barrier to linearity, which leads to an abrupt change from smooth to kinked variations in the v quantized (continuous lines) and n quantized (dashed lines) energy levels around the position of this maximum. Quantitative differences between figures 2 and 3 in the vibrational energy level spacings and in the shapes of the smooth continuous and dashed curves depend of course on the nature of the potential surface.

A third example, illustrated in figure 4, is taken from the spherical pendulum model for dipolar pendular states. The discussion in the appendix shows that three possible labelling schemes may be employed in this case—each involving the conserved angular momentum projection, m, onto the z axis. Points in each vertical ladder may be ascribed successive polar quantum numbers $v_\theta = 0, 1, 2, \ldots$, but the degenerate oscillator label $n = 2v_\theta + |m|$ is strongly preferred for small amplitude oscillations of the pendulum. The smooth quadratic variation with m at given n is then seen to go over to the characteristic kinked shape at energies above the barrier to end-over-end rotation; the dashed curves, which are kinked at low energies and smooth at energies

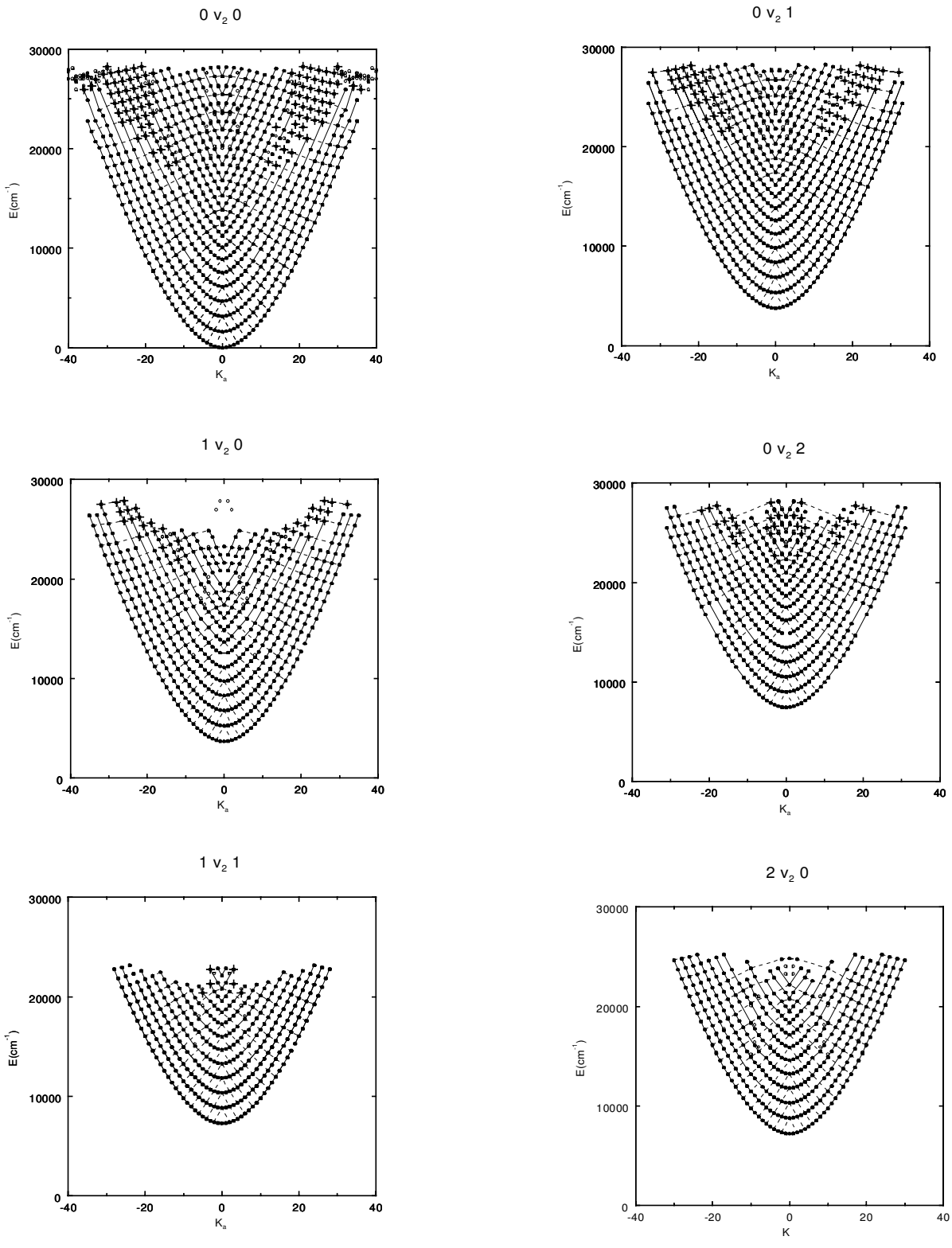

Figure 3. Monodromy plots of various computed bending progressions of water taken from the data of Partridge and Schwenke [14]. The rotational energies are taken for the J_{J0} states; hence $K_a = J$. The solid circles, which are joined by solid and dashed lines as in figure 2, display the monodromic pattern. Those with superimposed crosses (+) have been reassigned with respect to v_2 (see text). Open circles indicate reported, usually extra, states [14] that do not conform with the pattern.

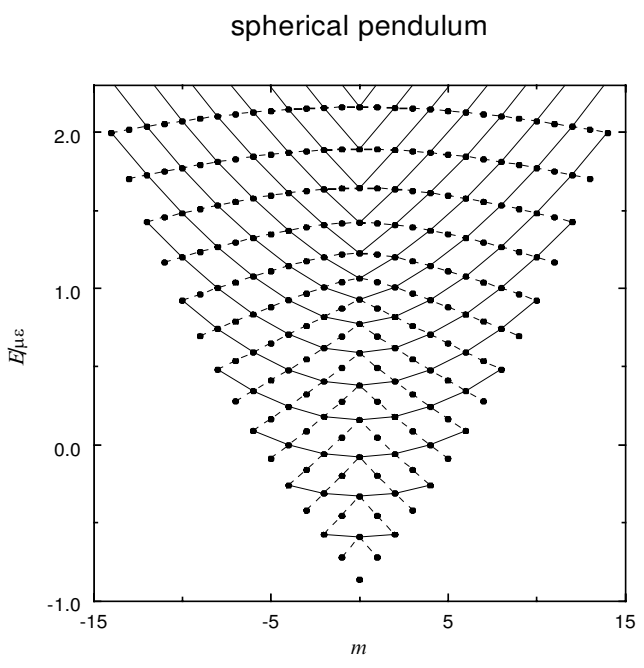

Figure 4. The computed quantal spectrum for the spherical pendulum model with $\mu\mathcal{E}/B = 100$. Points indicate the computed eigenvalues, which are labelled upwards from zero in each column by v_θ. m is the z component of angular momentum. Solid and dashed lines join those with common values of the pendulum quantum number $n = 2v_\theta + |m|$ and the rotational quantum number $j = v_\theta + |m|$ respectively. Note the abrupt transition from smooth to kinked variations in both sets of curves around the critical point at $m = 0$, $E/\mu\mathcal{E} = 1$.

above the barrier, are those with a common rotational label $j = v_\theta + |m|$. The main qualitative features again carry over from figures 2 and 3.

3. Semiclassical interpretation

The semiclassical origin of the monodromy in figures 1 and 2 may be derived from the Bohr quantization condition for the champagne bottle model (see appendix).

$$\frac{1}{h}\int_{R_{\min}}^{R_{max}} p_R(E, K; R)\,\mathrm{d}R = \left[v(E, K) + \frac{1}{2}\right]\pi, \qquad (2)$$

where $R_{\min}$ and $R_{\max}$ are the classical turning points, given by zeros of the radial momentum

$$p_R(E, K; R) = \{2m[E - (K^2\bar{h}^2/2mR^2) + AR^2 - BR^4]\}^{1/2}. \qquad (3)$$

The partial derivative identity

$$(\partial E/\partial K)_v = -(\partial v/\partial K)_E / (\partial v/\partial E)_K \qquad (4)$$

is first employed to examine the derivatives of the continuous curves in figure 2 at $K = 0$, taking care to recognize that the function $v(E, K)$ is non-analytic at the critical point $(K, E) = (0, 0)$, due to confluence of the inner turning point $R_{\min}$ with the singularity at $R = 0$ (see the appendix for a more detailed discussion).

The energy derivative at $K = 0$ reduces to

$$\left(\frac{\partial v}{\partial E}\right)_{K=0} = \frac{2}{h}\int_{R_{\min}}^{R_{\max}} \frac{m\,\mathrm{d}R}{p_R(E, 0; R)} = \frac{1}{h}\oint \frac{\mathrm{d}R}{\dot{R}} = \frac{T_{\mathrm{vib}}}{h}, \qquad (5)$$

where T_{vib} is the classical time period of the vibration. Corrections to the Bohr–Sommerfeld rule due to a logarithmic divergence of T_{vib} as $|E| \to 0$ are shown elsewhere [13] to diminish rapidly away from the critical point. It was also found that T_{vib} is approximately symmetric with respect to the sign of E over a wide energy region.

The angular momentum derivative

$$\left(\frac{\partial v}{\partial K}\right)_E = \frac{K\bar{h}}{\pi}\int_{R_{\min}}^{R_{\max}} \frac{\mathrm{d}R}{R^2\{2m[E - (K^2\bar{h}^2/2mR^2) + AR^2 - BR^4]\}^{1/2}} \qquad (6)$$

must be treated with care. It is zero for $K = 0$ and $E < 0$ because the integral is finite. However the integral diverges as $|K|^{-1}$ for $E > 0$ because $R_{\min} \to 0$ as $K \to 0$ and different branches of the square root must be taken according to the sign of K. The presence of this branch point of $v(K, E)$ at $E = 0$, $K = 0$ lies at the heart of the monodromy. Its physical origin may be demonstrated by use of the semiclassical identity $K\bar{h} = mR^2\dot{\theta}$, where $\dot{\theta}$ is the angular velocity; thus equation (6) may be re-expressed as

$$\left(\frac{\partial v}{\partial K}\right)_E = \frac{1}{2\pi}\int_{R_{\min}}^{R_{\max}} \frac{\dot{\theta}}{\dot{R}}\,\mathrm{d}R = -\frac{1}{2\pi}\oint \dot{\theta}\,\mathrm{d}t = -\frac{\Delta\theta}{2\pi}, \qquad (7)$$

where $\Delta\theta$ is the polar angle change during a vibrational cycle. The limiting value as $K = 0$ is readily deduced from the forms of the negative and positive energy trajectories in figures 5(*a*) and (*b*) respectively. $\Delta\theta = 0$ for $E < 0$ and $\Delta\theta = \pm\pi$ for $E < 0$ according to the sign of K. Hence

$$\left(\frac{\partial v}{\partial K}\right)_E = \begin{cases} 0, & E < 0, \\ -\frac{1}{2}, & E > 0, K > 0, \\ \frac{1}{2}, & E > 0, K < 0. \end{cases} \qquad (8)$$

Equation (8), which explains the sharp transition from a smooth continuous curve at $K = 0, E < 0$ in figure 2 to a kink when $E > 0$, is seen from the trajectory diagram to depend solely on the presence of a cylindrically sym-

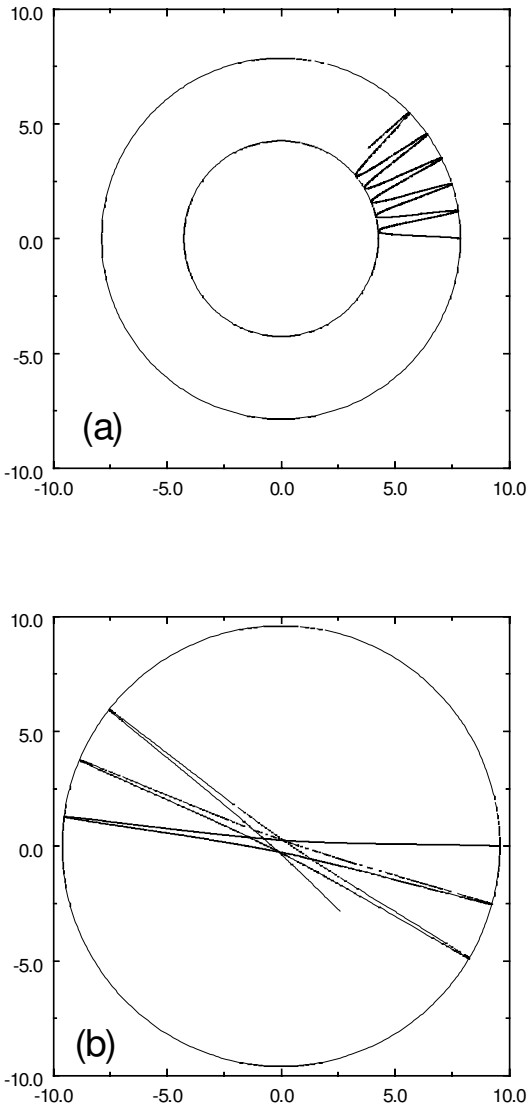

Figure 5. Classical trajectories for the scaled champagne-bottle model with $\beta = 0.00625$, $\kappa = 1$ and (*a*) $E = -7.5$, (*b*) $E = 7.5$. Note that the total angular change for one vibrational cycle reduces to zero in the limit $\kappa \to 0$ in panel (*a*), but to $\pm\pi$, according to the sign of κ in panel (*b*). Secondly the opposite senses of precession in the two panels should be noted.

metric maximum in the potential function; the precise functional form is irrelevant.

The behaviour of the dashed curves, linking points with linear molecule quantum numbers $\ell = \kappa$ and $n = 2v + |\ell|$ is also readily explained. Their derivatives are given by

$$(\partial E/\partial \ell)_n = -(\partial n/\partial \ell)_E/(\partial n/\partial E)_\ell, \tag{9}$$

where $(\partial n/\partial E)_\ell = 2(\partial v/\partial E)_\kappa$; while in accordance with (8)

$$\left(\frac{\partial n}{\partial \ell}\right)_E = \frac{\partial}{\partial K}(2v \pm \kappa) = \begin{cases} +1, & E < 0, \ell = \kappa < 0, \\ -1, & E < 0, \ell = \kappa > 0, \\ 0, & E > 0. \end{cases} \tag{10}$$

The kinks in the continuous curves at $\ell = 0$ and $E > 0$ have been transferred to kinks in the dashed ones at $E < 0$. It is also evident from equations (4), (5), (8), (9) and (10) that the slopes of the two sets of kinked curved (dashed and continuous) have a mirror symmetry around the barrier maximum to the extent that $T_{\text{vib}}(E) \simeq T_{\text{vib}}(-E)$.

The positive and negative curvatures of the continuous (constant v) and dashed (constant n) curves are related elsewhere [13] to the positive and negative precessional rates of the negative and positive energy trajectories in figure 5.

4. Discussion and conclusions

Monodromy would appear to have important consequences for the structure of the energy levels of quasi-linear molecules, of which we have taken water as a possible example. To observe monodromy in water it would be necessary to assign spectra with at least 10 quanta of bending excitation. Published spectra only go half this far [17], although recent work has extended the assignment to the $(0,6,0)$ band [18]. Furthermore, analysis of sunspot spectra [15] and near infrared laboratory spectra [16] has extended the assignments to levels with 7 quanta of bending excitation in combination with excited stretching states. As there remain many unassigned transitions, particularly in the sunspot spectra, it seems likely that higher bending states will be analysed soon.

Other systems may also be considered, because water has a relatively high barrier to linearity and may not therefore seem the most likely candidate in a search for monodromy. Moreover the selection rules for transitions within the electronic ground state are much less favourable for the observation of long progressions than those involving electronic excitation. On the other hand many well known excited states of quasi-linear molecules are complicated by electronic degeneracies and the consequent Renner–Teller non-adiabatic coupling. The present single-surface approach to the analysis is therefore inappropriate. Other candidates include single-surface, quasi-linear molecules, such as C_3O_2 [19] and HNCO [20], for which bending spectra have been recorded. However it would appear that the systems analysed to date either have nonlinear minima too shallow to support a significant number of bending states below the monodromy point, as is the case for C_3O_2 and HNCO [21], or that the observed spectra do

not yet extend to the monodromy point, as is the case for H_2O. No firm experimental evidence for this interesting effect is therefore yet available.

As indicated in the introduction, the plots in figures 2–4 are in one sense simply presentations of known results in quasi-linear molecule theory [6, 7]. We have however stressed the generality of the abrupt change in level structure about the monodromy point, for all systems with cylindrically symmetric potential barriers. The relationship between these abrupt changes and the forms of relevant classical trajectories was strictly demonstrated only for the two-dimensional champagne bottle and spherical pendulum models but the similarity with the fully coupled computed results for water was strikingly evident. It remains to be seen whether this is merely evidence of a rather weak interaction between the bending and stretching modes in this particular molecule, but since the freedom to pass through linearity is associated with the vanishing of one moment of inertia, it seems likely that the monodromy will prove to be a persistent effect. No doubt perturbations will occur in most molecules at energies as high as 25 000 cm^{-1} but use of the double $|v_2, \kappa_2\rangle$, $|n_2, \ell_2\rangle$ grid employed in figures 2–4 is expected to be a powerful aid to assignment.

The authors are grateful to Professor Richard Cushman for drawing their attention to this interesting problem and to CCP6 for support. Helpful discussions with G. G de Polavieja, B. P. Winnewisser and M. Winnewisser are gratefully acknowledged. TW is grateful for an EPSRC research assistantship.

Appendix: analytical considerations

The mathematical origin of the monodromy is illustrated below by reference to the champagne bottle system. Analytical aspects of the more complicated spherical pendulum system are also addressed.

A.1. *Champagne bottle*

The κ structure associated with high amplitude bending states of a bent molecule is modelled by the 'champagne bottle' [13] Hamiltonian, with the classical form

$$H = \frac{1}{2m}\left(p_R^2 + \frac{p_\phi^2}{R^2}\right) - A R^2 + B R^4. \qquad (A\,1)$$

Angular momentum is conserved, with $p_\phi = \kappa \hbar$ in quantum mechanics, and the quantum mechanical eigenvalues are readily obtained from an expansion in degenerate harmonic oscillator states [22]. The present analytical discussion starts by transforming equation (2) to the scaled form adopted in the earlier paper†

$$v(\kappa, \epsilon) + \frac{1}{2} = \frac{1}{2\pi}\int_{z_2}^{z_1} z^{-1}(2\epsilon z - z^2 + 2\beta z^3 - \kappa^2)^{1/2}\,dz \qquad (A\,2)$$

in which $z = (2mA/\hbar^2)^{1/2} R^2$, $\epsilon = (m/2A\hbar^2)^{1/2} E$, $\beta = (\hbar^2/8mA^3)^{1/2} B$ while z_1 and z_2 are the turning points. The monodromy arises from a confluence of the inner turning point with the singularity as $\kappa \to 0$ and it follows from equation (54) of [13] that $v(\kappa, \epsilon)$ contains a turning point contribution of the form

$$f(\kappa, \epsilon) = -\frac{1}{2\pi}\left[\kappa \arctan\left(\frac{\epsilon}{\kappa}\right) + \frac{\epsilon}{2}\ln\left(\frac{\epsilon^2 + \kappa^2}{4}\right) + \frac{|\kappa|\pi}{2}\right]$$
$$= -\frac{1}{2\pi}\left[\mathrm{Im}\left\{(\kappa + i\epsilon)\ln\left(\frac{\kappa + i\epsilon}{2}\right)\right\} + \frac{|\kappa|\pi}{2}\right]. \qquad (A\,3)$$

It is evident from equation (A 3) that $v(\kappa, \epsilon)$ has a logarithmic singularity at $\kappa = \epsilon = 0$.

The nature of the monodromy in figure 1 can also be traced to the multivalued nature of the arctangent contribution to $f(\kappa, \epsilon)$. The numbering given in the diagram corresponds to choice of the principal value, $-\pi/2 < \arctan(\epsilon/\kappa) < \pi/2$, but equation (A 3) implies that $v(\kappa, \epsilon) \to v(\kappa, \epsilon) - \kappa$ if the arctangent is allowed to pass smoothly to the next sheet after an anticlockwise cycle around the origin. Conversely the energy ϵ must be increased to that of the original point $[\kappa, v(\kappa, \epsilon) + \kappa]$ if the quantum number $v(\kappa, \epsilon)$ is conserved during the cycle. Consequently the vector $(\Delta\kappa, \Delta v)$ between points labelled $[\kappa_i, v_i]$ and $[\kappa_j, v_j]$ in figure 1 evolves to the vector $(\Delta\kappa, \Delta v + \Delta\kappa)$ around such a $v(\kappa, \epsilon)$ preserving cycle, which accords exactly with equation (1).

Equation (A 3) also has implications for the derivative $(\partial v/\partial\kappa)_\epsilon$ as $\kappa \to 0$, which was analysed pictorially in section 3. Thus

$$\lim_{\kappa \to 0_\pm}\left(\frac{\partial f}{\partial \kappa}\right) = -\frac{1}{2\pi}\left[\pm\arctan\left(\frac{\epsilon}{\kappa}\right) \pm \frac{\pi}{2}\right]. \qquad (A\,4)$$

The terms on the right hand side cancel for $\epsilon < 0$ and combine to give $\pm\frac{1}{2}$ for $\epsilon > 0$. Hence the limits of $(\partial v/\partial\kappa)_\epsilon$ implied by equations (A 3) and (A 4) coincide with those given by equation (8).

† These scaling relations are unfortunately incorrect in the earlier paper [13].

A.2. *Spherical pendulum*

The pendular motions of a diatomic molecule with dipole μ and rotational constant B in an electric field $\mathcal{E}$ are governed by the Hamiltonian

$$H = BJ^2 - \mu\mathcal{E}\cos\theta = B\left(p_\theta^2 + \frac{p_\phi^2}{\sin^2\theta}\right) - \mu\mathcal{E}\cos\theta. \qquad (A\,5)$$

The angular momentum component $p_\phi = m\hbar$ is again conserved and the quantum mechanical Hamiltonian is readily diagonalized in a spherical harmonic basis. The semiclassical situation has an additional complication, compared with the earlier model, that the following Bohr–Sommerfeld quantization condition may involve confluences between either of the classical turning points, θ_1 and θ_2, and the singularities at $\theta = \pi$ and $\theta = 0$ respectively:

$$v_\theta + \frac{1}{2} = \frac{1}{h}\oint p_\theta\,\mathrm{d}\theta = \frac{2}{h\,B^{1/2}}\int_{\theta_2}^{\theta_1}(E + \mu\mathcal{E}\cos\theta - m^2\hbar^2/\sin^2\theta)^{1/2}\,\mathrm{d}\theta. \qquad (A\,6)$$

The coalescence at $\theta = \pi$ is responsible for the monodromy in figure 4, while that at $\theta = 0$ has consequences for the limiting behaviour of $(\partial v_\theta/\partial m)_\epsilon$ as $m \to 0$. The analysis is simplified by the substitutions $a = E/\mu\mathcal{E}$, $b = \hbar(B/\mu\mathcal{E})^{1/2}$ and $z = \cos\theta$, which reduce equation (A 6) to the form

$$v_\theta + \frac{1}{2} = \frac{1}{\pi b}\int_{z_2}^{z_1}\frac{(-z^3 - az^2 + z - b^2m^2)^{1/2}}{(1 - z^2)}\,\mathrm{d}z. \qquad (A\,7)$$

Thus

$$\left(\frac{\partial v_\theta}{\partial m}\right)_\epsilon = -\left(\frac{bm}{2\pi}\right)(I_+ - I_-), \qquad (A\,8)$$

where

$$I_\pm = \int_{z_2}^{z_1}\frac{\mathrm{d}z}{(z \pm 1)(-z^3 - az^2 + z - b^2m^2)^{1/2}} = \frac{2}{(z_1 \pm 1)(z_1 - z_3)^{1/2}}\Pi\left(\frac{z_1 - z_2}{z_1 \pm 1}, \left(\frac{z_1 - z_2}{z_1 - z_3}\right)^{1/2}\right). \qquad (A\,9)$$

The notation in equation (A 9) has $z_1 > z_2 > z_3$ for the roots of the cubic polynomial, while $\Pi(\alpha^2, k)$ is the complete elliptic integral of the third kind, in the notation of Gradsteyn and Ryzhik [23]. A careful examination of the behaviour of the roots z_i as $m \to 0_\pm$, coupled with the identity [24]

$$\Pi(\alpha^2, k) = -\Pi(k^2/\alpha^2, k) + K(k) + \frac{\pi}{2}\left[\frac{\alpha^2}{(1 - \alpha^2)(\alpha^2 - k^2)}\right]^{1/2} \qquad (A\,10)$$

leads to the conclusion that I_+ is finite for $E < \mu\mathcal{E}$ but diverges as $\pi/b|m|$ for $E > \mu\mathcal{E}$, while I_- diverges as $-\pi/b|m|$ for all E. Consequently

$$\lim_{m \to 0_\pm}\left(\frac{\partial v_\theta}{\partial m}\right)_E = \begin{cases} \mp\frac{1}{2}, & \text{for } E < \mu\mathcal{E}, \\ \mp 1, & \text{for } E > \mu\mathcal{E}. \end{cases} \qquad (A\,13)$$

It follows that the labels $n = 2v_\theta + |m|$ and $j = v_\theta + |m|$ used for the continuous and dashed lines in figure 5 respectively are defined in such a way that $(\partial n/\partial m)_E = 0$ for $E < \mu\mathcal{E}$ and $(\partial j/\partial m)_E = 0$ for $E > \mu\mathcal{E}$. The analogues of the partial derivative identity in equation (4) therefore ensure that $(\partial E/\partial m)_n = 0$ for $E < \mu\mathcal{E}$ and $(\partial E/\partial m)_j = 0$ for $E > \mu\mathcal{E}$.

References

[1] Hazewinkel, M., 1994, *Encyclopaedia of Mathematics* (Reidel: Kluwer Academic).
[2] Marsden, J. E., and Hoffman, M. J., 1987, *Basic Complex Analysis* (New York: Freeman).
[3] Solari, A. G., Natiello, M. A., and Minplin, G. B., 1996, *Non-linear Dynamics* (Bristol: Institute of Physics).
[4] (*a*) Bates, L. R., 1991, *J. Appl. Math. Phys.* (*ZAMP*), **42,** 837; (*b*) Cushman, R., 1983, *Centruumvoor Wiskd. Inf. Newslett.,* **1,** 4.
[5] Friedrich, B., 1995, *Int. Rev. Phys. Chem.,* **14,** 113.
[6] Dixon, R. N., 1964, *Trans. Faraday Soc.,* **60,** 1363.
[7] Johns, J. W. C., 1967, *Can. J. Phys.,* **45,** 2639.
[8] Potts, A. W., and Price, W. C., 1972, *Proc. Roy. Soc.* (Lond) A, **326,** 181.
[9] Jungen, Ch., and Merer, A. J., 1980, *Molec. Phys.,* **40,** 1.
[10] Dixon, R. N., Duxbury, G., Horani, M., and Rostas, J., 1971, *Molec. Phys.,* **22,** 977.
[11] Duxbury, G., Jungen, Ch., and Rostas, J., 1983, *Molec. Phys.,* **48,** 719.
[12] Karlsson, L., Mattson, L., Jadrny, R., Bergmark, T., and Seigbarn, K., 1976, *Phys. Scripta,* **13,** 229.
[13] Child, M. S., 1998, *J. Phys.* A, **31,** 657.
[14] Partridge, H., and Schwenke, D. W., 1996, *J. chem. Phys.,* **106,** 4618.
[15] Polyansky, O. L., Zobov, N. F., Viti, S., Tennyson, J., Bernath, P. F., and Wallace, L., 1997, *Astrophys. J.,* **489,** L205.

[16] Polyansky, O. L., Zobov, N. F., Viti, S., and Tennyson, J., 1998, *J. molec. Spectrosc.*, **189,** 291.
[17] Polyansky, O. L., Zobov, N. F., Tennyson, J., Lotoski, J. A., and Bernath, P. F., 1997, *J. molec. Spectrosc.*, **184,** 35.
[18] Zobov, N. F., Polyanski, O. L., Tennyson, J., Lotoski, J. A., Colarusso, P., Zhang, K.-Q., and Bernath, P. F., 1999, *J. Mol. Spectrosc.* (in press).
[19] Walters, A. D., Winnewisser, M., Lattner, K., and Winnewisser, B. P., 1991, *J. molec. Spectrosc.,* **149,** 542.
[20] Preusser, J., Schermel, R., Winnewisser, M., and Winnewisser, B. P., 1996, *J. molec. Spectrosc.,* **176,** 99.
[21] Handy, N. C., Murray, C. W., and Amos, R. D., 1994, *Phil. Mag.* B, **69,** 755.
[22] Wilson, E. B., Decius, J. C., and Cross, P. C., 1954, Molecular Vibrations: the Theory of Infrared and Raman Spectra (New York: McGraw-Hill).
[23] Gradsteyn, J. S., and Ryzhik, I. M., 1965, Tables of Integrals, Series and Products (New York: Academic Press).
[24] Byrd, P. F., and Friedman, M. D., 1971, Handbook of Elliptic Integrals for Engineers and Scientists, 2nd Edn (Berlin: Springer-Verlag).